Available online at www.sciencedirect.com
SCIENCE DIRECT
Journal of Solid State Chemistry 179 (2006) 1588–1595
JOURNAL OF SOLID STATE CHEMISTRY
www.elsevier.com/locate/jssc

Crystal chemistry and crystallography of the SrR_2CuO_5 (R = lanthanides) phases

W. Wong-Ng[a,*], T. Haugan[b], J.A. Kaduk[c], R.A. Young[d], Z. Yang[a], M.H. Jang[a], M. Luong[e]

[a]*Ceramics Division, National Institute of Standards and Technology (NIST), A256 MATLS, 100 Bureau Dr., Stop 8520, Gaithersburg, MD 20899, USA*
[b]*AFRL, Wright-Patterson AFB, OH 45433, USA*
[c]*BP Chemicals, Naperville, IL 60566, USA*
[d]*Physics Department, Georgia Institute of Technology, Atlanta, GA 30332, USA*
[e]*Chemistry Department, University of Maryland, MD 20742, USA*

Received 27 October 2005; received in revised form 24 January 2006; accepted 27 January 2006
Available online 20 March 2006

Abstract

The crystal chemistry and crystallography of the compounds SrR_2CuO_5 (Sr-121, R = lanthanides) were investigated using the powder X-ray Rietveld refinement technique. Among the 11 compositions studied, only R = Dy and Ho formed the stable SrR_2CuO_5 phase. SrR_2CuO_5 was found to be isostructural with the "green phase", BaR_2CuO_5. The basic structure is orthorhombic with space group *Pnma*. The lattice parameters for $SrDyCuO_5$ are $a = 12.08080(6)$ Å, $b = 5.60421(2)$ Å, $c = 7.12971(3)$ Å, $V = 482.705(4)$ Å^3, and $Z = 8$; and for the Ho analog are $a = 12.03727(12)$ Å, $b = 5.58947(7)$ Å, $c = 7.10169(7)$ Å, $V = 477.816(9)$ Å^3, and $Z = 8$. In the SrR_2CuO_5 structure, each R is surrounded by seven oxygen atoms, forming a monocapped trigonal prism (RO_7). The isolated CuO_5 group forms a distorted square pyramid. Consecutive layers of prisms are stacked in the *b*-direction. Bond valence calculations imply that residual strain is largely responsible for the narrow stability of the SrR_2CuO_5 phases with R = Dy and Ho only. X-ray powder reference diffraction patterns for $SrDy_2CuO_5$ and $SrHo_2CuO_5$ were determined.

Keywords: Crystal chemistry of SrR_2CuO_5 (R = lanthanides)

1. Introduction

In recent years, promising properties of the high T_c superconductor coated conductors prepared by depositing $Ba_2RCu_3O_{6+x}$ (213, R = lanthanides and Y) on substrates using either the ion beam assisted deposition (IBAD) process [1,2] or the rolling assisted biaxial texturing substrates (RABiT) process [3,4] have renewed research interest in the entire 213 series, including the $Sr_2RCu_3O_{6+x}$ (Sr-213) phases. The Sr-213 phase is not stable under ambient conditions, but can be stabilized either under high pressure [5], or when Cu of the basal Cu–O chain site in the structure is partially or completely replaced by other appropriate metals [6,7].

Since Ba and Sr are both alkaline-earth elements, studies of the phase equilibria of SrR_2CuO_5 systems may provide further understanding of the crystal chemistry of the alkaline-earth lanthanide cuprates in general. Across the lanthanide series, the ionic radius of the lanthanide ions decreases, known as "lanthanide contraction". The crystal chemistry of various compounds can be interpreted as related to this trend. For example, in the $SrO-\frac{1}{2}R_2O_3-CuO$ systems, when R is large, the system consists of a larger number of solid solutions, and the diagram is simpler when the size of R is small [8,9]. There is a dramatic change of the diagrams near the CuO corners as R progresses from the largest La analog [10], through the Nd analog [11], to the smaller Ho- [12], Y- [13], and Yb-systems [14].

The compound BaY_2CuO_5 (Ba-121), commonly known as the "green phase", is an impurity often found coexisting with the high T_c superconductor phase, $Ba_2YCu_3O_{6+x}$.

*Corresponding author. Fax: +1 301 975 5334.
E-mail address: Winnie.wong-ng@nist.gov (W. Wong-Ng).

0022-4596/$ - see front matter © 2006 Elsevier Inc. All rights reserved.
doi:10.1016/j.jssc.2006.01.079

The structure of this green phase has been studied by the powder X-ray diffraction method [15], and by single crystal diffraction methods [16,17]. The powder diffraction patterns of the lanthanide substituted BaR_2CuO_5 phases, with R = Sm, Gd, Dy, Ho, Er, Tm, Yb and Lu, have been measured by Wong-Ng et al. [18]. The cell parameters of these green phases show a trend as a function of the ionic size of R, which suggests isomorphism of the lanthanide phases with the Y compound. In the Ba-system, the "green phase" BaR_2CuO_5 forms with all R^{3+} ions from Sm to Lu.

This investigation is part of an ongoing project to understand the crystal chemistry and phase equilibria in the $AO-\frac{1}{2}R_2O_3-CuO$ (A = Ba, Sr) systems [18–22]. The main goal of this paper is to study the trend of phase formation and crystal chemistry of the SrR_2CuO_5 phase as a function of the size of R [8,9], and also the phase equilibria in the vicinity of the SrR_2CuO_5 (Sr-121) phase in the $BaO-\frac{1}{2}R_2O_3-CuO$ system. The crystallography of the SrR_2CuO_5 phases was studied using the X-ray diffraction Rietveld refinement method [23]. Since the X-ray powder diffraction technique is of primary importance for phase characterization, extensive coverage and reference diffraction patterns of superconductors and related phases in the International Centre for Diffraction Data (ICDD) Powder Diffraction File (PDF) [24] are critical for the scientific community. Another goal of this paper is to report the X-ray reference patterns for the SrR_2CuO_5 series of compounds.

2. Experimental[1]

2.1. Sample preparation

About 1 g each of the 11 polycrystalline samples of the SrR_2CuO_5 compositions, where R = La, Nd, Sm, Eu, Gd, Dy, Ho, Er, Y, Yb, Tm, Lu were prepared using the high-temperature solid-state sintering method. Well-mixed stoichiometric powders of $SrCO_3$, R_2O_3, and CuO were compacted by pressing the powder in a pelletizing die. The compacted powders were heated in air according to the schedule of 850 °C for 2 d, and 950 °C for 9 d. Each time after the samples were taken out of the furnace, they were reground and repelletized.

2.2. Powder X-ray diffraction

2.2.1. Experimental X-ray diffraction

X-ray powder diffraction was used to identify the phases synthesized and to confirm single phase purity. A computer-controlled automated diffractometer equipped with a theta-compensation slit and Cu$K\alpha$ radiation was used at 45 kV and 40 mA. The radiation was detected by a scintillation counter and solid state amplifier. The Siemens software package and the reference X-ray diffraction patterns of the ICDD PDF were used for performing phase identification.

2.2.2. Rietveld refinements

For Rietveld refinement studies and reference pattern measurements, the SrR_2CuO_5 compounds were ground as acetone slurries in a mortar and pestle. The slurries were placed on zero-background cells and allowed to dry. A Bruker D8 Advance diffractometer equipped with a VÅNTEC-1 position-sensitive detector was used to measure the patterns (Cu$K\alpha$ radiation, 40 kV, 40 mA). Patterns were measured from 5° to 140° 2θ in 0.00729689° steps, counting for 0.2 or 2 s/step.

The initial studies of the two compounds were conducted using the DBWS program PC version 9807a [25,26]. The preliminary structural model used was that of $BaHo_2CuO_5$ [27]. During the final detailed structural characterization and preparation of standard reference patterns for submission to the PDF [24], the General Structure Analysis System (GSAS) [28] was employed. For the Rietveld refinements, only the 12–140° portions of the patterns were used. Soft constraints of 2.34(5) Å were applied to the R–O bonds. The basal Cu–O bonds of the CuO_5 distorted pyramid were restrained to 1.95(2) Å, and the axial Cu–O bond to 2.17(2) Å. The restraints contributed <1% to the final reduced χ^2. Common isotropic displacement coefficients were refined by atom type. The Ho sample contained 1.1 wt% Ho_2O_3 and 10.2 wt% $Ho_2Cu_2O_5$ as impurities; the Dy sample contained 2.3 wt% Dy_2O_3. The phase fractions of each phase were refined, as well as the lattice parameters. Second-order spherical harmonic preferred orientation terms were refined for the SrR_2CuO_5 phases, but the texture indices were very small. The profiles were described by the Thompson–Cox–Hastings pseudo-Voigt function (Profile function #2). Only the X size broadening terms and a common specimen displacement coefficient were refined. The backgrounds were described by a 6- or 9-term shifted Chebyshev function of the first kind.

2.2.3. Powder pattern determination from GSAS

X-ray reference powder patterns of SrR_2CuO_5 were obtained with a Rietveld pattern decomposition technique. These patterns represent ideal specimen patterns. They are corrected for systematic errors both in d-spacing and intensity. The reported peak positions are calculated from the refined lattice parameters, as this represents the best measure of the true positions. For peaks resolved at the instrument resolution function, the individual peak positions are reported. For overlapping peaks, the intensity-weighted average peak position is reported with multiple indices. For marginally resolved peaks, individual peaks are reported to more accurately simulate the visual appearance of the pattern.

[1]The purpose of identifying the equipment in this article is to specify the experimental procedure. Such identification does not imply recommendation or endorsement by the National Institute of Standards and Technology.

3. Results and discussion

3.1. Phase formation of SrR_2CuO_5

Table 1 shows the results of X-ray analysis of 11 SrR_2CuO_5 compositions prepared at 950 °C. Unlike the Ba-analogs where BaR_2CuO_5 can be prepared for all stable R^{3+} ions, it was found that in the Sr-analog only R = Ho, and Dy form this green phase (despite with a small amount of impurity phases). The ionic radii of these ions are in the mid-range of the lanthanide series. The Sr-121 compositions with larger and smaller lanthanide ions lie in a three-phase region in the phase diagram as indicated by the X-ray results. It is seen that along the R_2O_3–CuO binary system, when R = Nd, Sm, Eu, and Gd, the R_2CuO_4 phase is formed, while when R is relatively small, namely with Dy, Ho, Y, Er, Yb, Tm, and Lu, the $R_2Cu_2O_5$ phase is formed. Fig. 1 shows a blown-up portion of the lower angle part of the X-ray diffraction pattern of $SrHo_2CuO_5$, with *hkl* indices of selected strong peaks indicated.

Table 1
X-ray analysis results for SrR_2CuO_5

R	Phases present	Reference
La	La_2O_3, SrO, $(Sr,La)_2CuO_x$	[10]
Nd	Nd_2O_3, $Sr_{1.7}Nd_{1.3}Cu_2O_6$, $Sr_{1.2}Nd_{0.8}CuO_{4-y}$	[11]
Sm	Sm_2O_3, $Sr_{1.7}Sm_{1.3}Cu_2O_6$, $SrSm_2O_4$	This work
Eu	Eu_2O_3, $SrEu_2O_4$, $(Sr,Eu)_{14}Cu_{24}O_{41}$	This work
Gd	Gd_2O_3, $SrGd_2O_4$, $(Sr,Gd)_{14}Cu_{24}O_{41}$	This work
Dy	$SrDy_2CuO_5$	This work
Ho	$SrHo_2CuO_5$	This work
Y	Y_2O_3, Y_2SrO_4, $(Sr,Y)_{14}Cu_{24}O_{41}$	This work
Er	$Sr_2Cu_2O_5$, $SrEr_2O_4$, $(Sr,Er)_{14}Cu_{24}O_{41}$	This work
Tm	$Sr_2Cu_2O_5$, $SrTm_2O_4$, $(Sr,Tm)_{14}Cu_{24}O_{41}$	This work
Yb	$Sr_2Cu_2O_5$, $SrYb_2O_4$, $(Sr, Yb)_{14}Cu_{24}O_{41}$	[14]
Lu	$Sr_2Cu_2O_5$, $SrLu_2O_4$, $(Sr,Lu)_{14}Cu_{24}O_{41}$	This work

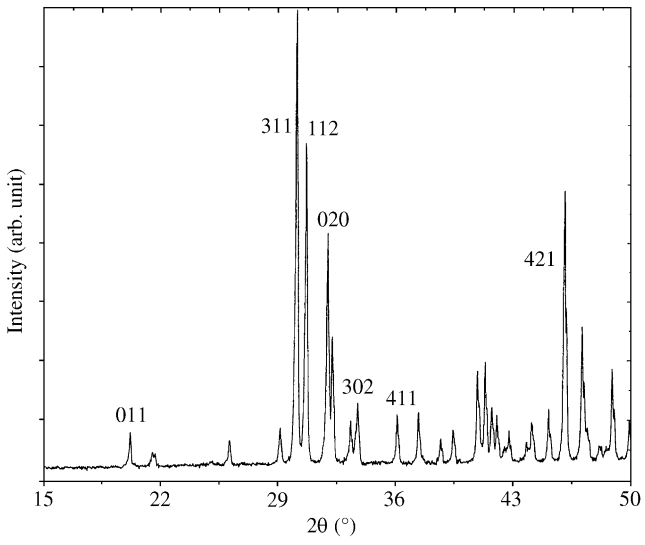

Fig. 1. X-ray diffraction pattern of $SrHo_2CuO_5$ showing selected *hkl* indices.

Table 2
Refined global parameters for SrR_2CuO_5, R = Dy and Ho

	Dy	Ho
Specimen displacement	−7.80(1)	6.84(3)
Profile X	7.17(2)	7.36(3)
P. O. Spherical harmonics		
200	−0.095(5)	0
202	−0.153(4)	0
Texture index	1.007	1.000
wR_p	0.0114	0.0424
R_p	0.0084	0.0329
$R(F)$	0.0341	0.0504
$R(F^2)$	0.0535	0.0821
χ^2	2.074	1.793
ΔF, $\pm$, e/Å^3	1.6/−2.3	2.9/−1.9
# Variables	40	37
# Observations	17 559	17 005

The refined global parameters of Rietveld refinements of SrR_2CuO_5 are shown in Table 2, including the final refinement residuals, wR_p, R_p, $R(F)$ and $R(F^2)$. Fig. 2 shows the typical profile fit and difference patterns for $SrHo_2CuO_5$ as an example. This diagram shows the observed, calculated and difference X-ray powder patterns. The observed and difference patterns are plotted at the same scale. In the section with $2\theta > 70°$, the vertical scale is multiplied by 10. The rows of tick marks indicate the calculated peak positions; the first row is for the impurity phase Ho_2O_3, the second row is for $Ho_2Cu_2O_5$, and the third one is for the main phase, $SrHo_2CuO_5$. Residual differences between observed and calculated profiles are probably the result of incomplete powder averaging.

3.2. Lattice parameters of SrR_2CuO_5

Both SrR_2CuO_5 compounds crystallize in space groups *Pnma*. The lattice parameters a, c and V all decrease as Dy is substituted by the smaller Ho. The lattice parameters for $SrDyCuO_5$ are $a = 12.08080(6)$ Å, $b = 5.60421(2)$ Å, $c = 7.12971(3)$ Å, $V = 482.705(4)$ Å^3, and $Z = 8$; and for the Ho analog are $a = 12.03727(12)$ Å, $b = 5.58947(7)$ Å, $c = 7.10169(7)$ Å, $V = 477.816(9)$ Å^3, and $Z = 8$.

3.3. Structure of $SrDy_2CuO_5$ and $SrHo_2CuO_5$

Table 3 gives the atomic coordinates and displacement coefficients for $SrDy_2CuO_5$ and $SrHo_2CuO_5$. These compounds are confirmed to be isostructural to the Ba-121 "green phase" [15–17,19]. Bond distances of $SrDy_2CuO_5$ and $SrHo_2CuO_5$ are listed in Table 4.

The basic structure of SrR_2CuO_5 consists of RO_7, SrO_{10} and CuO_5 polyhedra. The lanthanide ion is 7-fold coordinated inside a monocapped trigonal prism, and two such units are joined to form the basic structure motif, R_2O_{11} (Fig. 3). Fig. 4 shows the discrete 5-fold coordinated

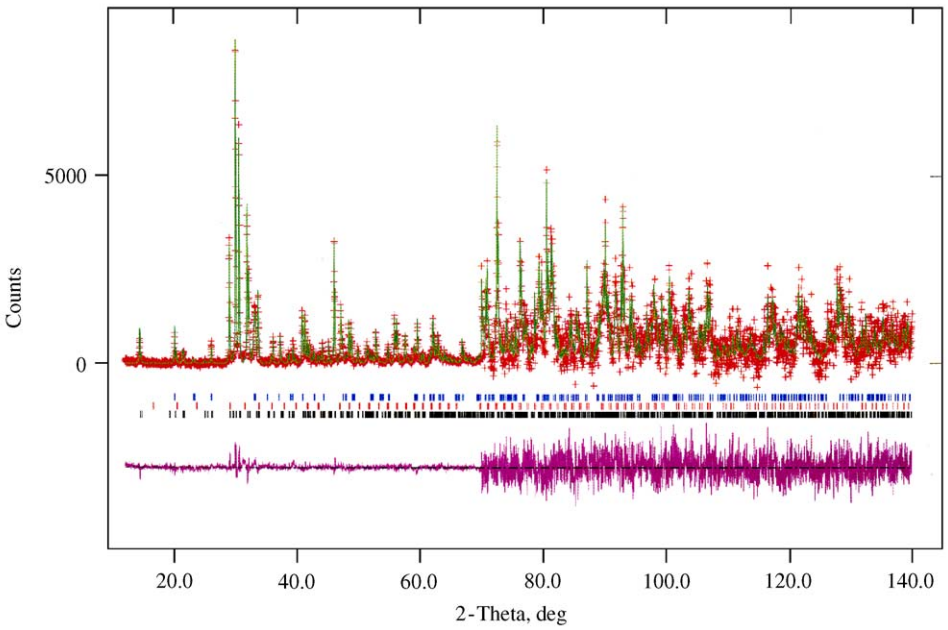

Fig. 2. The observed, calculated and difference patterns (plotted at the same scale) for $SrHo_2CuO_5$. The row of tick marks indicates the calculated peak positions (first row: impurity phase Ho_2O_3; second row: impurity phase $Ho_2Cu_2O_5$; and the third row: $SrHo_2CuO_5$). The intensity "I" is expressed in arbitrary units. The observed and difference patterns are plotted at the same scale. In the section with $2\theta > 70^\circ$, the vertical scale is multiplied by 10.

Table 3
Refined atomic coordinates and displacement coefficients for $SrHo_2CuO_5$ and $SrDy_2CuO_5$

Atom	x	y	z	U_{iso} (Å^2)
(1) $SrDy_2CuO_5$				
Sr1	0.9134(1)	1/4	0.9280(2)	0.0149(4)
Dy2	0.28749(6)	1/4	0.1157(1)	0.0081(3)
Dy3	0.07347(8)	1/4	0.3936(1)	0.0081
Cu4	0.6591(2)	1/4	0.7127(2)	0.0057(5)
O5	0.4357(5)	−0.0125(8)	0.1798(5)	0.0211(9)
O6	0.2290(4)	0.5091(8)	0.3487(9)	0.0211
O7	0.0854(7)	1/4	0.0677(8)	0.0211
(2) $SrHo_2CuO_5$				
Sr1	0.9112(2)	1/4	0.9265(3)	0.0145(6)
Ho2	0.2879(1)	1/4	0.1158(2)	0.0191(3)
Ho3	0.0732(1)	1/4	0.3936(2)	0.0191
Cu4	0.6610(3)	1/4	0.7126(4)	0.0039(8)
O5	0.4372(6)	−0.0137(11)	0.1751(9)	0.017(2)
O6	0.2289(6)	0.5091(12)	0.3512(12)	0.017
O7	0.0955(9)	1/4	0.0672(11)	0.017

square pyramids of CuO_5. Consecutive layers of trigonal prisms are stacked in the b-direction at about 2.8 Å intervals (half of the b-axis), sharing trigonal faces. In Fig. 5, the projection of the lanthanide-oxygen motif blocks at $z = \frac{1}{4}$ is shown. These trigonal prisms share edges to form wave-like chains parallel to the long z-axis. Chains are cross-linked by copper ions. Sr ions are found inside cages formed by four units of R_2O_{11} motif. The observed Sr–O contact distances cover a broad range of values. A total of nine Sr–O distances are found between 2.30 and 2.94 Å, while the tenth and eleventh Sr–O distances are 3.10 and 3.17 Å in the Dy-analog and 3.07 and 3.20 Å in the Ho-analog, respectively. These large distances suggest that the cage in which Sr^{2+} resides is very distorted.

Table 4
Bond distances (Å) in $SrHo_2CuO_5$ and $SrDy_2CuO_5$

$SrHo_2CuO_5$		$SrDy_2CuO_5$	
Sr1–O5 × 2	3.205(6)	Sr1–O5 × 2	3.171(4)
Sr1–O5 × 2	2.874(8)	Sr1–O5 × 2	2.869(6)
Sr1–O6 × 2	2.924(9)	Sr1–O6 × 2	2.945(6)
Sr1–O6 × 2	3.066(9)	Sr1–O6 × 2	3.099(6)
Sr1–O7	2.433(12)	Sr1–O7	2.305(9)
Sr1–O7 × 2	2.796(0)	Sr1–O7 × 2	2.802(0)
Ave.	2.924	Ave.	2.916
BVS	1.493	BVS	1.652
Ho2–O5 × 2	2.362(8)	Dy2–O5 × 2	2.362(6)
Ho2–O6 × 2	2.323(8)	Dy2–O6 × 2	2.317(6)
Ho2–O6 × 2	2.321(8)	Dy2–O6 × 2	2.342(6)
Ho2–O7	2.343(11)	Dy2–O7	2.465(8)
Ave.	2.336	Ave.	2.358
BVS	3.004	BVS	2.953
Ho3–O5 × 2	2.399(6)	Dy3–O5 × 2	2.439(4)
Ho3–O5 × 2	2.256(6)	Dy3–O5 × 2	2.282(5)
Ho3–O6 × 2	2.388(5)	Dy3–O6 × 2	2.396(4)
Ho3–O7	2.334(8)	Dy3–O7	2.328(6)
Ave.	2.346	Ave.	2.358
BVS	2.967	BVS	2.912
Cu4–O5 × 2	1.944(5)	Cu4–O5 × 2	1.916(5)
Cu4–O6 × 2	1.943(5)	Cu4–O6 × 2	1.960(4)
Cu4–O7	2.138(6)	Cu4–O7	2.189(5)
Ave.	1.983	Ave.	2.988
BVS	2.246	BVS	2.242

BVS is the bond valence sum [29,30].

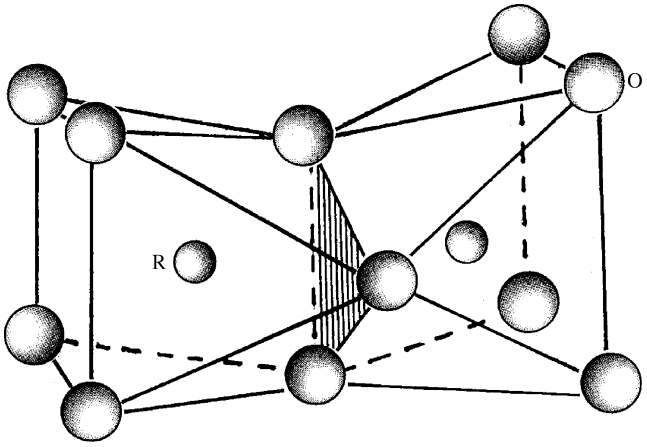

Fig. 3. Seven-fold coordination of R in SrR_2CuO_5 (R = Dy, Ho) is shown inside a monocapped trigonal prism. Two such RO_7 units are joined to form the basic structure motif of R_2O_{11} [15,17].

3.4. Bond valence calculations

It is a general practice to use the bond valence technique, which was developed by Brown and Altermatt [29], to calculate the atomic valence of the cations to evaluate the possible site residual strain. The bond valence sum, BVS, of an atom i is defined as the sum of the bond valences v_{ij} of all the bonds from atom i to atoms j. The commonly adopted empirical expression for the bond valence v_{ij} as a function of the interatomic distance d_{ij} is $v_{ij} = \exp[(r_0 - d_{ij})/B]$. The parameter B is commonly taken to be a "universal" constant equal to 0.37 Å. Values of the reference distance r_0 are tabulated for various pairs of atoms [30].

In Table 4, the BVSs, are given. The BVS values for Cu in both compounds are greater than 2 (2.25 for $SrHo_2CuO_5$ and 2.24 for $SrDy_2CuO_5$). The deviations from the valence

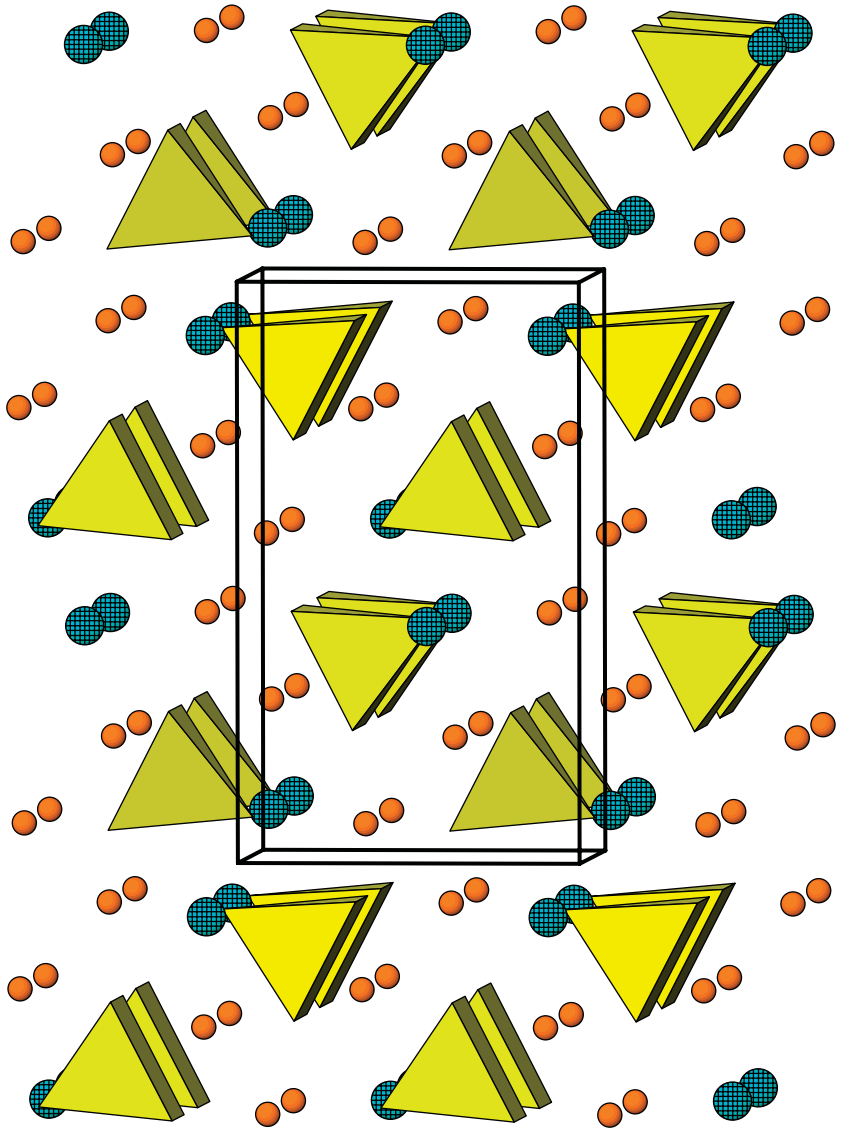

Fig. 4. Discrete 5-fold coordinated square pyramids of CuO_5 in the unit cell of SrR_2CuO_5. The structure is viewed along b-axis, the large and small spheres are used to represent Sr and R, respectively.

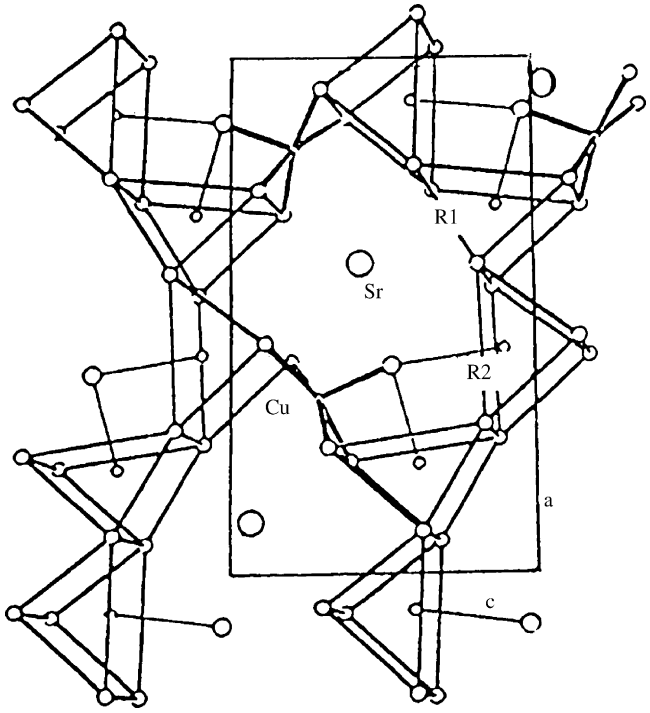

Fig. 5. Projection of the structure of SrR_2CuO_5 in the (010) plane of the linkage of R_2O_{11} polyhedra (one layer), showing one layer of the wavelike chains along the *a*-axis [17,19].

sum rule suggests that the structure contains residual bond strain. Cu is overbonded, or Cu in the CuO_5 distorted "square pyramid" is experiencing a compressive strain. On the other hand, the BVS values for Sr in both compounds are substantially less than 2, namely, 1.49 for $SrHo_2CuO_5$ and 1.65 for $SrDy_2CuO_5$. Sr is underbonded and is in tensile stress, or the Sr–O cages are relatively large in the structure. According to Brown and Altermatt [29], large residual strain could cause instability of the structure. If the Sr-121 type compound can be prepared for lanthanide size smaller than that of Ho, the tensile residual strain for Sr would be greater than the stability limit, with an expected value of BVS < 1.49.

There are two independent *R*'s in the unit cell. The lanthanides in these seven-coordinated cages do not appear to experience a significant amount of strain, as suggested by the bond valence values in Table 3, which are close to the value of 3. However, from the projected trend for *R*2 (i.e., 2.97 for the Ho-analog, and 2.91 for Dy), the BVS value could be smaller, or the residual strain for these lanthanide cages could be greater, for compounds with lanthanide ionic size greater than that of Dy. Therefore, based on the BVS values for both Sr, *R*2 and Cu, the SrR_2CuO_5 structure type is only stable for the Ho and Dy analogs.

Table 5
X-ray diffraction pattern for $SrHo_2CuO_5$ (orthorhombic *Pnma*, $a = 12.03727(12)$ Å, $b = 5.58947(7)$ Å, $c = 7.10169(7)$ Å, $V = 477.816(9)$ Å^3, and $Z = 8$)

d	*I*	*h*	*k*	*l*	*d*	*I*	*h*	*k*	*l*	*d*	*I*	*h*	*k*	*l*
6.11657	83	1	0	1	6.01866	15	2	0	0	4.39227	86	0	1	1
4.12616	26	1	1	1	4.09571	29	2	1	0	3.40578	48	1	0	2
3.05829	26	2	0	2	3.00933	5	4	0	0	2.96242	999*	3	1	1
2.90841	727	1	1	2	2.79477	487	0	2	0	2.77083	264	4	0	1
2.68295	70	2	1	2	2.65913	43	3	0	2	2.64971	96	4	1	0
2.48254	82	4	1	1	2.40125	84	3	1	2	2.38730	5	2	2	1
2.32276	40	1	0	3	2.28002	82	5	0	1	2.20297	126	2	0	3
2.19613	22	0	2	2	2.17982	145	0	1	3	2.16047	81	1	2	2
2.14493	58	1	1	3	2.12362	17	4	1	2	2.11114	44	5	1	1
2.06308	24	2	2	2	2.04886	67	2	1	3M	2.04886	67	4	2	0M
2.00622	70	6	0	0	1.96768	390	4	2	1	1.93066	7	6	0	1
1.92645	181	3	2	2	1.91541	45	3	1	3	1.88828	14	6	1	0
1.86058	118	4	0	3	1.82487	51	6	1	1	1.80219	7	0	3	1
1.77544	62	0	0	4	1.76646	42	5	2	1M	1.76646	42	4	1	3M
1.75643	18	1	0	4	1.74671	29	6	0	2	1.73011 108	2	2	3	
1.67565	28	1	1	4	1.67132	40	7	0	1	1.64398	158	3	3	1
1.63457	129	1	3	2	1.62978	28	6	2	0	1.61587	8	5	1	3
1.60127	14	7	1	1	1.59115	13	2	3	2	1.58849	7	6	2	1
1.58413	14	4	3	0	1.54876	121	4	2	3	1.54614	16	4	3	1
1.52994	12	6	0	3M	1.52994	12	4	0	4M	1.52589	20	3	3	2
1.50467	19	8	0	0	1.49861	39	0	2	4	1.49156	153	7	1	2
1.48713	16	1	2	4	1.48121	51	6	2	2	1.47495	98	4	1	4
1.47199	6	8	0	1	1.46409	43	0	3	3	1.45307	48	1	3	3M
1.45307	48	8	1	0M	1.44273	9	5	3	1	1.43440	23	7	2	1
1.42294	15	8	1	1M	1.42294	15	2	3	3M	1.41056	6	1	0	5
1.39738	79	0	4	0	1.39128	32	7	0	3	1.38438	14	5	1	4
1.37660	17	0	1	5	1.37539	9	3	3	3	1.36524	5	6	3	0
1.35394	6	7	2	2	1.34240	11	6	2	3	1.34069	15	6	3	1
1.33894	6	3	0	5	1.32956	25	6	0	4	1.32486	17	8	2	0
1.30210	80	3	1	5	1.29310	9	6	1	4M	1.29310	9	1	4	2M
1.27948	12	9	1	1	1.27806	8	1	3	4	1.25926	12	1	2	5

Table 5 (*continued*)

d	*I*	*h*	*k*	*l*	*d*	*I*	*h*	*k*	*l*	*d*	*I*	*h*	*k*	*l*
1.24769	35	4	4	1	1.24549	14	7	2	3	1.24412	5	7	3	1
1.23830	15	8	1	3	1.23698	10	3	4	2	1.20751	7	3	2	5
1.20612	30	7	1	4	1.20062	21	6	2	4	1.19062	72	5	4	1M
1.19062	72	7	3	2M	1.18362	8	0	0	6	1.18202	38	4	3	4
1.18001	28	2	4	3	1.17675	17	10	1	0	1.17061	14	8	3	0
1.14788	6	8	0	4	1.14665	14	6	4	0	1.13526	14	3	0	6
1.13385	6	5	3	4	1.12956	10	0	3	5	1.12066	6	5	2	5
1.11734	38	4	4	3	1.09807	20	0	4	4	1.09510	6	7	0	5
1.09353	6	1	4	4	1.09239	17	10	2	1	1.09117	11	6	4	2
1.08991	25	0	2	6	1.08730	51	3	3	5	1.08547	9	1	2	6
1.08154	5	11	0	1	1.07402	8	9	3	1	1.07298	28	10	0	3
1.07204	16	7	4	1	1.06472	37	3	5	1	1.06197	53	1	5	2+
1.05180	27	3	2	6	1.04932	7	8	3	3	1.04577	13	11	0	2
1.03671	6	4	5	1	1.03286	6	8	0	5	1.03054	5	3	5	2
1.02952	18	7	3	4	1.02393	12	8	4	0	1.01957	19	7	2	5M
1.01957	19	6	0	6M	1.01097	21	10	3	0+	1.00865	5	11	2	1
1.00169	47	10	2	3	0.99822	16	0	1	7	0.99273	5	1	4	5
0.98593	22	7	4	3	0.98068	17	10	1	4M	0.98068	17	3	5	3M
0.97944	34	11	2	2	0.97793	7	12	1	1	0.96882	16	8	2	5
0.96677	5	3	4	5	0.96323	19	6	4	4	0.96137	17	4	0	7
0.96049	28	7	1	6	0.95771	19	6	2	6	0.95067	7	1	2	7
0.94309	7	1	5	4	0.93848	9	10	2	4	0.93537	15	11	3	1
0.93159	16	0	6	0	0.92210	6	5	1	7	0.92044	6	5	4	5
0.90909	19	4	2	7	0.90623	33	7	5	2	0.90317	10	0	4	6
0.90246	20	4	5	4	0.89735	8	8	5	0	0.89371	5	6	1	7
0.89101	10	0	3	7	0.88699	8	8	4	4	0.88469	18	13	1	2
0.88300	43	4	6	1+	0.88113	22	3	4	6	0.88046	5	5	5	4
0.87920	13	3	6	2	0.87855	17	10	3	4M	0.87855	17	0	5	5M
0.87648	7	12	3	1	0.87441	16	1	1	8	0.86386	24	7	3	6
0.86210	14	5	6	1M	0.86210	14	7	4	5M	0.85981	10	14	0	0
0.85810	51	3	5	5M	0.85810	51	2	6	3M	0.85662	41	11	1	5
0.85529	8	11	4	1	0.85156	6	9	5	1	0.85104	38	10	4	3
0.84562	5	5	4	6	0.84494	7	6	6	0	0.84379	13	14	1	1
0.84174	26	4	1	8	0.83909	8	8	5	3	0.83727	24	11	4	2
0.83561	6	5	3	7	0.83301	33	4	6	3	0.83182	11	8	1	7

3.5. Powder diffraction patterns for $SrDy_2CuO_5$ and $SrHo_2CuO_5$

Reference patterns for $SrDy_2CuO_5$ and $SrHo_2CuO_5$ were submitted to ICDD for inclusion in the PDF. Table 5 shows the pattern for the $SrHo_2CuO_5$ phase. The *d*-spacing values are given along with the Miller indices and integrated intensities, which were normalized to the value 999 as the maximum. The symbols M and + refer to peaks containing contributions from two reflections, and more than two reflections, respectively.

4. Summary

In summary, the trend of phase formation of SrR_2CuO_5 in the $SrO-\frac{1}{2}R_2O_3-CuO$ systems was studied. Unlike the Ba-analogs in which the 121 phases can be prepared for all *R*'s with stable 3+ valence, among the 12 compositions of SrR_2CuO_5 prepared, only the $R = Dy$ and Ho compositions formed the stable 121 green phase. The structure of $SrDy_2CuO_5$ and $SrHo_2CuO_5$ were studied by the Rietveld refinement technique and were found to be isostructural to BaR_2CuO_5. From bond distance and bond valence calculations, possible reasons for the instability of other analogs appear to be due to the high distortion of Sr–O, Cu–O and *R*–O cages. X-ray powder patterns were prepared and submitted to the PDF.

References

[1] S.R. Foltyn, E.J. Peterson, J.Y. Coulter, P.N. Arendt, Q.X. Jia, P.C. Dowden, M.P. Maley, X.D. Wu, D.E. Peterson, J. Mater. Res. 12 (1997) 2941–2946.
[2] Y. Iijima, N. Tanabe, O. Kohno, Y. Ikeno, Appl. Phys. Lett. 60 (6) (1992) 769–771.
[3] A.P. Malozemoff, S. Annavarapu, L. Fritzemeier, Q. Li, V. Prunier, M. Rupich, C. Thieme, W. Zhang, A. Goyal, M. Paranthaman, D.F. Lee, Supercond. Sci. Technol. 13 (2000) 376–473.
[4] A. Goyal, D.F. Lee, F.A. List, E.D. Specht, R. Feenstra, M. Paranthaman, X. Cui, S.W. Lu, P.M. Martin, D.M. Kroeger, D.K. Christen, B.W. Kang, D.P. Norton, C. Park, D.T. Verebelyi, J.R. Thompson, R.K. Williams, T. Aytug, C. Cantoni, Physica C 357 (2001) 903.
[5] B. Okai, Jpn. J. Appl. Phys. 29 (1990) L2180.
[6] T. Den, T. Kobayashi, Physica C 196 (1992) 141.

[7] J.T. Vaughey, J.P. Theial, E.F. Hasty, D.A. Groenke, L. Stern, K.R. Poeppelmeier, B. Dabrowski, D.G. Hinks, A.W. Mitchell, Chem. Mater. 3 (1991) 935.
[8] R.D. Shannon, C.T. Prewitt, Acta Crystallogr. 25 (1969) 925–946.
[9] R.D. Shannon, Acta Crystallogr. A 32 (1976) 751–767.
[10] D.M. DeLeeuw, J. Less-Common Metal. 150 (1989) 95–107.
[11] X. Chen, J. Liang, C. Wang, G. Rao, X. Xing, Z. Song, Z. Qiao, J. Alloy. Compd. 205 (1–2) (1994) 101.
[12] W. Wong-Ng, Q. Huang, I. Levin, J.A. Kaduk, J. Dillingham, T. Haugan, J. Suh, L.P. Cook, Int. J. Inorg. Mater. 3 (2001) 1283.
[13] R.S. Roth, C.J. Rawn, J.D. Whitler, C.K. Chiang, W. Wong-Ng, J. Am. Ceram. Soc. 72 (3) (1998) 395.
[14] J. Dillingham, W. Wong-Ng, I. Levin, Int. J. Inorg. Mater. 3 (2001) 569.
[15] C. Michel, B. Raveau, J. Solid State Chem. 43 (1982) 73–80.
[16] S.F. Watkins, F.R. Fronczek, K.S. Wheelock, R.G. Goodrich, W.O. Hamilton, W.W. Johnson, Acta Crystallogr. C 44 (1988) 3–6.
[17] W. Wong-Ng, M.A. Kuchinski, H.F. McMurdie, B. Paretzkin, Powder Diff. 4 (1) (1989) 2.
[18] W. Wong-Ng, B. Paretzkin, E.R. Fuller Jr., Adv. X-ray Anal. 33 (1989) 453.
[19] R.M. Hazen, L.W. Finger, R.A. Angel, C.T. Prewitt, N.L. Ross, H.K. Mao, C.G. Hadidiacos, Phys. Rev. B 35 (1987) 7238.
[20] W. Wong-Ng, B. Paretzkin, E.R. Fuller Jr., J. Solid State Chem. 85 (1990) 117.
[21] W. Wong-Ng, L.P. Cook, M.D. Hill, B. Paretzkin, E.R. Fuller Jr., Crystal chemistry and phase equilibrium studies of the BaO ($BaCO_3$)–R_2O_3–CuO systems. V. Melting relations in Ba_2(Y,Nd,Eu)-Cu_3O_{6+x}, in: D. Christen, J. Narayan, L. Schneemeyer (Eds.), High-Temperature Superconductors: Fundamental Properties and Novel Materials Processing, vol. 169, Material Research Society, Pittsburgh, PA, 1990, p. 81.
[22] W. Wong-Ng, P. Paretzkin, Powder Diff. 6 (4) (1991) 187.
[23] H.M. Rietveld, J. Appl. Crystallogr. 2 (1969) 65–71.
[24] PDF, Powder Diffraction File produced by ICDD, 12 Campus Blvd., Newtown Square, PA 19073-3273.
[25] R.A. Young, A.C. Larson, C.O. Paiva-Santos, PROGRAM DBWS-9907a for Rietveld Analysis of X-ray and Neutron Powder Diffraction Patterns, School of Physics, Georgia Institute of Technology, Atlanta, GA 30332, May 1999. Copyright R.A. Young, 1999.
[26] R.A. Young, The Rietveld Method, International Union of Crystallography, Oxford University Press, Oxford, 1995 (pp. 1–38).
[27] A. Salinas-Sanchez, J.L. Garcia-Muñoz, J. Rodriguez-Carvajal, R. Saez-Puche, J.L. Martinez, J. Solid State Chem. 100 (1992) 201–211.
[28] A.C. Larson, R.B. von Dreele, GSAS—General Structure Analysis system, US Government contract (W-7405-ENG-36) by the Los Alamos National laboratory, which is operated by the University of California for the U.S. Department of Energy, 1992.
[29] I.D. Brown, D. Altermatt, Acta Crystallogr. B 41 (1985) 244–247.
[30] N.E. Brese, M. O'Keeffe, Acta Crystallogr. B 47 (1991) 192.